This is an open access article published under a Creative Commons Attribution (CC-BY) License, which permits unrestricted use, distribution and reproduction in any medium, provided the author and source are cited.

Article

Cite This: *Biomacromolecules* 2019, 20, 1719−1730

pubs.acs.org/Biomac

Active Modulation of States of Prestress in Self-Assembled Short Peptide Gels

Henry Cox,[†] Meiwen Cao,[§] Hai Xu,[§] Thomas A. Waigh,*[,†,‡] and Jian R. Lu*[,†]

[†]Biological Physics, School of Physics and Astronomy and [‡]Photon Science Institute, University of Manchester, Oxford Road, Manchester M13 9PL, U.K.

[§]Centre for Bioengineering and Biotechnology, China University of Petroleum (East China), 66 Changjiang West Road, Qingdao 266580, China

Supporting Information

ABSTRACT: Peptide hydrogels are excellent candidates for medical therapeutics due to their tuneable viscoelastic properties, however, in vivo they will be subject to various osmotic pressures, temperature changes, and biological co-solutes, which could alter their performance. Peptide hydrogels formed from the synthetic peptide I_3K have a temperature-induced hardening of their shear modulus by a factor of 2. We show that the addition of uncross-linked poly(*N*-isopropylacrylamide) chains to the peptide gels increases the gels' temperature sensitivity by 3 orders of magnitude through the control of osmotic swelling and cross-linking. Using machine learning combined with single-molecule fluorescence microscopy, we measured the modulation of states of prestress in the gels on the level of single peptide fibers. A new self-consistent mixture model was developed to simultaneously quantify the energy and the length distributions of the states of prestress. Switching the temperature from 20 to 40 °C causes 6-fold increases in the number of states of prestress. At the higher temperature, many of the fibers experience constrained buckling with characteristic small wavelength oscillations in their curvature.

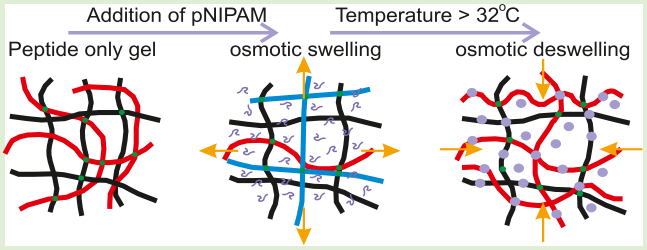

INTRODUCTION

Gels are complex materials, expressing a range of designer viscoelastic properties, which a solid or liquid alone cannot deliver. This kind of mechanical response is particularly desirable in medical therapeutics, as gels can be used to mimic biological tissue, such as in tissue engineering and wound healing.[1,2] Through the addition of complementary chemical modifications or polymers, the functionality of these materials can be greatly enhanced.[3] For example, cross-links can be formed using enzymes[4] or by the addition of bridging biomolecules which support the gel structure.[5] The use of interpenetrating polymer networks has also been successful, and gel strengths in the MPa range have been achieved with adhesive properties to rival commercially available surgical alternatives.[6−8] The components of these gels, such as alginate mixed with polyacrylamide, work co-operatively to produce composite networks that have superior properties compared with each of the individual components and, although some partially successful theories exist, there is a lack of a detailed understanding on the single molecule level.

Peptide-based gels have gained significant interest commercially as they are formed from naturally occurring amino acids and are therefore biodegradable and often biocompatible.[9] Synthetic peptides can be designed to harness the properties of different amino acids and self-assemble through thermodynamically driven processes into large ordered structures.[10] Some of the most popular peptides self-assemble into long, thin fibrils which then cross-link and entangle, forming networks which trap water and provide mechanical strength.[10,11] The resulting macroscopic properties of these gels are determined by the physical interactions between the fibrils and, despite considerable research effort, there is not an accurate theory which describes such semiflexible polymeric gels.[7,12] The networks are complex, load-bearing structures, and researchers have demonstrated that changing a variety of environmental factors can yield large changes in their bulk properties.[13] These effects are commonly attributed to the modulation of cross-link strength between fibrils, such as changing the ion concentrations in the gel which alters the interfibre adhesive potentials. However, the load bearing structures lead to novel states of quenched disorder, such as states of prestress, which have important implications for the mechanical properties.[14−16]

We recently provided strong evidence that a significant portion of the semiflexible fibrils in gelled peptide networks is under prestress by comparing persistence length measurements from single-molecule dynamics and static images of the fibrils. We then applied a naive Bayesian mixture model to identify the population of fibrils under stress in the networks.[17] Thus, the modulation of stresses in the peptide networks provides an

Received: January 18, 2019
Revised: March 7, 2019
Published: March 13, 2019

© 2019 American Chemical Society

DOI: 10.1021/acs.biomac.9b00085
Biomacromolecules 2019, 20, 1719−1730

excellent opportunity to control the physical properties of these materials. More generally, the use of stresses to precondition biopolymer networks has already been demonstrated to modulate the network load-bearing capabilities on the macroscale, e.g., with collagen.[18] Here, we provide more fundamental information on the origin of the prestresses on the level of single peptide fibers through thermal, noncovalent modulation of the prestresses using the addition of poly(*N*-isopropylacrylamide) (pNIPAM).

pNIPAM is a popular polymer due to the temperature-induced coil-to-globule transition which occurs at its lower critical solution temperature (LCST), which is approximately 32 °C, near human body temperature.[19] This has led to much exciting research with thermoresponsive systems based on pNIPAM microgels and hybrid systems,[20−22] many of which exhibit large changes in volume above and below the LCST.[23] We recently developed a mixed peptide/pNIPAM gel system with potential for use as an injectable drug delivery system which undergoes a fully reversible sol−gel transition at near body temperature (∼32 °C), increasing the potential specificity of an incorporated drug.[24] Furthermore, the presence of pNIPAM did not appear to significantly affect the self-assembled peptide structures and it facilitated gelling at concentrations below the usual gelation concentration of the system, suggesting that it modulated the strength and number of cross-links in the networks. Atomic force microscopy (AFM), circular dichroism, and neutron scattering experiments were performed to analyze the self-assembled structures and bonds present, and the results were consistent with our previous work on peptide-only systems.[24,25] However, AFM results revealed bulges along the peptide fibrils predominantly at fiber junctions, suggesting that the pNIPAM stabilized the network by acting as a glue and provided additional cross-links.

In the present study, we investigated the dynamics of the peptide/pNIPAM system at the level of single fibers to show the underlying physical mechanisms behind this behavior. We used the synthetic surfactant-like peptide I_3K (I is isoleucine and K is lysine), which forms fibrils of radius ∼5 nm and lengths on the order of microns. The peptide is stable over long periods of time, easy to label with commercial fluorescent dyes and has been extensively characterized with a range of techniques, such as atomic force microscopy, neutron scattering, electron microscopy, and super-resolution fluorescence microscopy.[17,25−27] Furthermore, peptides, such as I_3K, are commercially relevant, as they are simple, inherently biocompatible, and have very short amino-acid sequences, making them cheaper to produce at scale with very high purity. We apply state-of-the-art microscopy and machine learning analysis techniques, including a self-consistent mixture model, to determine the states of prestress in the I_3K networks as a function of pNIPAM concentration and temperature. Using the self-consistent method allows us to determine the underlying length distributions of the stressed and unstressed fibrils within the sample. We conclude that in addition to modulating the strength of cross-links, the free pNIPAM chains apply osmotic pressure on the I_3K network, causing the gel to either swell or deswell, exerting tensional (swelling) and compressional (deswelling) stresses on the fibrils within it and a change in the elastic modulus of 3 orders of magnitude. Swelling/deswelling behavior is very common in pNIPAM-based systems following a first-order phase transition if the temperature is switched.[23] The addition of co-solutes can also cause the swelling of gels such as cross-linked DNA and has been explored in molecular dynamics simulations.[28,29]

These results are extremely significant for the performance of gels in therapeutic applications, and a 3 order of magnitude change in the modulus will also occur when the gel composites are placed in vivo due to the temperature increase in the gel. We quantified the underlying changes to the network on the level of individual fibrils, which provides crucial insights for systems of commercial importance.[30] Peptides, such as I_3K, are potential hosts for a range of drugs, such as antimicrobial peptides.[31] However, the properties of the networks themselves could be tuned using similar means to present a stress environment, which is favorable to the application. For example, reducing mechanical stresses in gels to prevent biofilm growth, which can render antimicrobial drugs ineffective.[32] From the perspective of fundamental research on polymer gels, this study represents the first evidence for the active modulation of states of prestress at the single molecule level and develops the understanding of these systems to allow more refined and rational design of functional materials based on semiflexible gels.[3]

MATERIALS AND METHODS

Sample Preparation. The water used in the experiments was sourced from a PURELAB purifier (18 MΩ). The I_3K peptides were synthesized using solid-phase FMOC synthesis, which ensures a high purity of >98%, as detailed in our previous work.[25] This peptide was from the same batch as previously used to demonstrate states of prestress in their networks.[17] Initially, peptide networks were formed by dissolving the I_3K in water to a peptide concentration of 20 mM. Dissolution was aided by sonication and heating to 40 °C for approximately 20 min. The peptides were then allowed to age for a week at room temperature.

For the fluorescence microscopy experiments, a partially labeled I_3K network was created. A sample of the peptides was labeled with Cy3B NHS Ester fluorescent dye obtained from GE Healthcare. The dye was predissolved in anhydrous-dimethyl sulfoxide to a concentration of 1 mg/mL. This was then mixed with the peptide to a final dye concentration of 20 μg/mL, and the conjugation reaction was allowed to complete on an orbital shaker for 2 h. Excess and unconjugated dye was removed from the sample by dialysis using a Slide-A-Lyzer MINI Dialysis Device from Thermo Scientific. Finally, the fully labeled peptides were then mixed with unlabeled peptides, such that 10% (v/v) of the peptide fibers was labeled and the rest was not. This process was necessary to reduce the background when imaging the samples with fluorescence microscopy.

The pNIPAM used was sourced from Sigma-Aldrich (M_w 20 000−40 000) and was predissolved in water to a concentration of 200 mg/mL. Furthermore, a 40 mM pH 4 acetic acid buffer was also prepared. The prepared buffer, I_3K (either partially labeled or unlabeled) and pNIPAM, were then all combined to form the final samples for experimentation. The samples were mixed gently but thoroughly, using a pipette and an orbital shaker to ensure that the pNIPAM and I_3K were distributed as evenly as possible through the samples.

Fluorescence Microscopy. The samples were mounted for imaging using microscope slides and circular imaging spacers (Thermo Scientific). Approximately, 7.5 μL of the sample was placed in the well formed by the spacer, and this was sealed in place using a circular coverslip. Fluorescence microscopy was performed on an Olympus IX71 microscope in an epi-illumination geometry with illumination provided by a 561 nm laser (Laser Quantum), which was delivered to the back of the microscope using an oscillated optical fiber. Fluorescence from the sample was collected using a Olympus UAPON 100XOTIRF oil immersion lens, and images were recorded using a Hamamatsu ORCA Flash v2 sCMOS camera. The high numerical aperture (1.49) of the lens allowed us to select thin 200 nm slices within the sample, and only fibrils which were aligned with this

DOI: 10.1021/acs.biomac.9b00085
Biomacromolecules 2019, 20, 1719−1730

imaging plane were used in the analysis. The camera was also able to record videos of fibril dynamics at 100 fps with a 10 ms exposure time. The positions of fibrils in the videos were tracked using the ImageJ plugin JFilament,[33] whereas in still images they were segmented using FiberApp.[34] Both software used open contour snakes algorithms to fit the position of the fibrils and more information on this procedure can be found in the Section 1 of the Supporting Information.

Rheology. Rheology experiments were performed on a Bohlin HR Nano rheometer fitted with a Julabo water bath and circulator to allow for temperature control. All experiments were performed using a cone-plate geometry with a cone which had an angle of 2°, a diameter of 20 mm, and a gap height set to 0.07 mm. This allowed a small amount of sample to be used in each experiment (approximately 110 μL) and for the system to reach thermal equilibrium in a short time. A solvent trap was used to minimize sample evaporation and, after loading, the sample was allowed to rest for 2 min to reach thermal equilibrium. Oscillatory rheology was performed on the samples, and a frequency sweep with controlled stress was performed in the range 0.1−10 Hz. The value of the controlled stress was determined by performing an amplitude sweep at 1 Hz, and the stress value for the frequency sweep was selected such that the sample was in the linear viscoelastic regime. Typical values for the stress used were between 0.02 and 5 Pa depending on the sample.

RESULTS AND DISCUSSION

Bulk Viscoelastic Properties. The self-assembling peptide I_3K was used throughout, and a 8 mM (4.2 mg/mL) peptide concentration was chosen as it is well above the critical micelle concentration of 0.43 mM for I_3K but low enough that the gel network formed was very soft.[25] We used a similar acetic acid buffer to our previous work on the dynamics of I_3K fibrils with a pH of 4 and a final buffer strength of 8 mM for all samples. This buffer was chosen to control the pH of the samples such that all of the fibrils were highly charged with weak cross-links and significant thermal dynamics. Other buffers were not chosen as they can cause the sample to precipitate, become too turbid for imaging or damp thermal dynamics such that they are no longer measurable.[26] In the hybrid I_3K/pNIPAM systems, three different pNIPAM concentrations were used: 1, 8, and 64 mg/mL. These were chosen to encompass a large range of concentrations while still allowing for microscopy to be performed at higher temperatures. Above the pNIPAM LCST, the globules of pNIPAM scattered light which rendered the sample increasingly opaque as the pNIPAM concentration was increased, which made fluorescence microscopy more challenging.

Samples used in the experiments are shown in Figure 1, where (A) and (C) were at room temperature (20 °C) and (B) and (D) were at an elevated temperature (40 °C). The left four samples in each image contain I_3K at 8 mM concentration, whereas the rightmost sample contains no I_3K. The pNIPAM concentrations of each sample were 0, 1, 8, 64, and 64 mg/mL from left to right in each image. Figure 1 demonstrates the simple effectiveness of the hybrid I_3K/pNIPAM system, as demonstrated in our other work.[24] When the peptide was not in the presence of pNIPAM, it did not form a self-supporting gel at either temperature, whereas when it was combined with pNIPAM, the thermoresponsive polymer strengthened the gel at high temperature and it became self-supporting. When pNIPAM was not in the presence of I_3K, it could not form a gelled structure and, although it transitioned from a clear to an opaque solution, the bulk mechanical properties did not change to the same extent as the hybrid system.

Rheology experiments were performed on the samples to quantify the visual changes in the bulk mechanical properties.

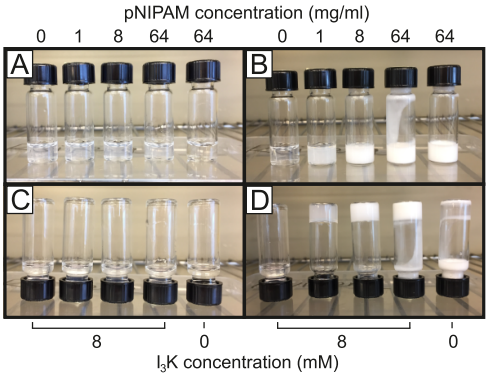

Figure 1. Images of the samples used in the study. In the left four samples in each image, there is 8 mM I_3K concentration with 0, 1, 8, and 64 mg/mL pNIPAM. In the rightmost sample of each image, there is just 64 mg/mL pNIPAM without any I_3K. The samples were imaged upright and inverted at 20 °C (A, C) and at 40 °C (B, D). All samples were not self-supporting at room temperature, but the combined effect of I_3K and pNIPAM strengthened the system which is self-supporting at the elevated temperature. In the 64 mg/mL pNIPAM samples (two rightmost vials), the high pNIPAM concentration caused moderate adhesion of the sample to the glass, and this effect was more pronounced when I_3K was included (second from the right).

Frequency sweeps in the range 0.1−10 Hz at constant stress were performed on the samples containing 8 mM I_3K and various pNIPAM concentrations at low and high temperatures, and the results are shown in Figure 2. The error bars on the measured elastic moduli shown in Figure 2A are calculated from the standard deviation of at least 12 repeats.

Figure 2A shows that even a small quantity of pNIPAM (1 mg/mL) reduces the mechanical strength of the system by approximately 1 order of magnitude at low temperatures (at a frequency of 1 Hz). Continued addition of pNIPAM to the system at the low temperature does not appear to significantly reduce the strength at the 1 Hz frequency, however it did have a more pronounced effect above the LCST temperature of pNIPAM. At high temperatures (40 °C) the addition of pNIPAM steadily increased the strength of the system and the 64 mg/mL pNIPAM with 8 mM I_3K is 2 orders of magnitude stronger than the 8 mM I_3K alone (4.6 kPa compared to 62 Pa at 1 Hz frequency). Given that the addition of pNIPAM weakens the system at lower temperatures, there was an active temperature-induced modulation in the strength of the gel by over 3 orders of magnitude for the 8 mM I_3K with 64 mg/mL pNIPAM sample, with the elastic modulus at 1 Hz frequency going from 1 Pa at 20 °C to 4.6 kPa at 40 °C.

To further analyze the rheology data, we fitted the frequency sweep data with a power law and expressed both the elastic and viscous moduli as power laws

$$G = G_o\omega^{\gamma} \quad (1)$$

where G_o is the plateau modulus, ω is the frequency, and γ is the scaling parameter.[35] Figure 2B,C shows the values of the plateau modulus and the scaling parameter for each sample and, the error bars were calculated using the co-variance matrix from the fitting procedure. The plateau modulus increased considerably with increasing pNIPAM concentration at the higher temperature, as expected from the data in Figure 2A. In contrast, the frequency scaling parameter, γ, was constant with the addition of pNIPAM at the higher temperature and was

DOI: 10.1021/acs.biomac.9b00085
Biomacromolecules 2019, 20, 1719−1730

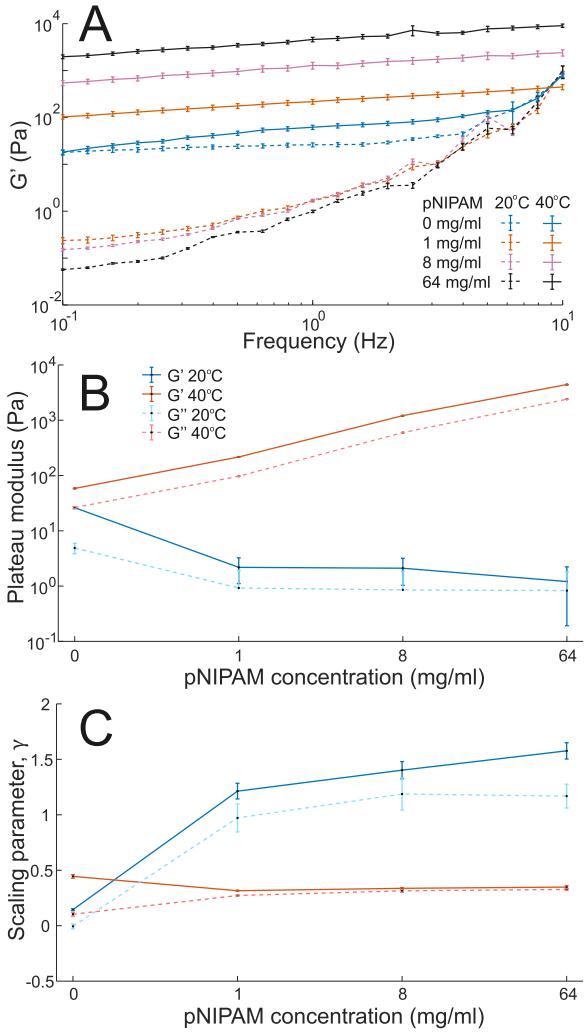

Figure 2. Summary of the linear oscillatory rheology data collected from each sample. (A) Frequency sweep data for the mean elastic modulus (G') of each sample, error bars are the standard error on the mean. At the low temperature, addition of pNIPAM lowered the elastic strength of the gel by approximately 1−2 orders of magnitude and also introduced a strong frequency dependence. At the higher temperature, the addition of pNIPAM strengthened the gel considerably and there is little frequency dependence. To compare the data further, a power law fit was performed on the data and the resulting plateau modulus and scaling parameter are shown in (B) and (C), respectively. The legend in (B) applies to (C) as well, and the errors are obtained from the variance of the fit parameters.

approximately 0.33 for the 1, 8, and 64 mg/mL pNIPAM with 8 mM I_3K samples i.e., the samples are weak power law gels.[35] At the lower temperature, the addition of pNIPAM to the I_3K system increases the scaling with frequency from 0.15 with 0 pNIPAM up to 1.2, 1.4, and 1.6 as the pNIPAM concentration increased through 1, 8, and 64 mg/mL.

In general, the bulk rheology experiments confirm the findings of our previous work,[24] and the qualitative conclusions we can draw from Figure 1. The relatively low scaling parameter, γ, for the samples at high temperature suggests that the system is gelled. Detailed studies of actin networks with transient cross-linkers have demonstrated similar power law rheology with $\gamma \sim 0.5$, which is modulated by the unbinding rate of the cross-linkers.[36] At the lower temperatures, the pNIPAM disrupts the cross-links of the I_3K network, as the system strength is more dependent upon the frequency, and the strength is greatly reduced compared to when there was no pNIPAM. This suggests that the sample is acting more like a solution of semiflexible filaments than a semiflexible gel network.[35] The underlying physical mechanism for the hardening/softening effects of pNIPAM is hard to deduce from the bulk rheology data alone. Intuitively, the rheology of the semiflexible I_3K fibril network will strongly depend upon the number and strength of cross-links between the fibrils. In our previous work, atomic force microscopy showed bulging around the peptide fiber junctions which indicated that the pNIPAM was interacting with the cross-links and enhancing their load bearing capabilities.[24]

Along with cross-link modulations, there are other factors that could affect the bulk properties, such as prestresses in the network which we recently showed to exist.[17] The phase behavior of pNIPAM has been well studied, and so it is worth considering the effect of the coil-to-globule transition of the pNIPAM on the I_3K/pNIPAM system.[37] One of the most significant changes to the pNIPAM is its volume. The radius of gyration of a pNIPAM coil ($M_w = 2 \times 10^5$) is a factor of 14 greater than the globule, which represents a reduction in the pervaded volume of over 3 orders of magnitude.[38] The I_3K and pNIPAM are combined after the preassembly of the I_3K fibrils and the formation of the network with gentle but thorough mixing ensuring that the I_3K fibrils are spread evenly. Therefore, in the coil state, the pNIPAM may swell the I_3K network slightly (an entropic stabilization effect), limiting interactions between I_3K fibrils and resulting in more solution-like viscoelastic properties. Swelling was investigated by measuring the mesh size of the I_3K network, but there was no statistically significant change in the results. As the pNIPAM transitions from coil to globule, the osmotic pressure from the pNIPAM is reversed, and the I_3K network is compressed. This forces the chains together and results in a stronger network, as has been seen for other compressed semiflexible polymer networks.[39] Adhesion of the pNIPAM chain onto the peptide chain may also lead to a stickier interfibre potential and thus additional cross-links with longer lifetimes.

Single-Molecule Dynamics of the System. To develop this model of the interaction between I_3K and pNIPAM, we considered single-molecule experiments to quantitatively investigate the dynamics of individual I_3K fibrils in the presence of pNIPAM. To capture the single-molecule dynamics, the I_3K fibrils were labeled with Cy3B fluorescent dye so that their position could be recorded using fluorescence microscopy. To reduce the signal to noise and isolate the dynamics of individual fibrils, a labeled sample was mixed with an identical unlabeled sample so that 1 in 10 fibrils was labeled. Videos of fibrils in each sample were recorded at 20 and 40 °C, and the position of the fibrils in each frame of the video were tracked using an open contour snakes algorithm with the ImageJ plugin JFilament.[33] More details of the tracking procedure can be found in the Section 1 of the Supporting Information.

A Fourier decomposition of each filament's shape was used to further analyze the dynamics of the filaments.[17,39,40] The tangent angle, θ, as a function of length along the fibril, s, was represented as a sum of cosines

DOI: 10.1021/acs.biomac.9b00085
Biomacromolecules 2019, 20, 1719−1730

$$\theta(s) = \sqrt{\frac{2}{L}} \sum_{n=1}^{\infty} a_q \cos(qs) \tag{2}$$

where each term in the sum corresponds to a wavevector, $q = \frac{n\pi}{L}$, n is the mode number, L is the length of the fibril, and a_q is the bending mode amplitude associated with the wavevector, q. The main advantages of this technique are that the cosine terms feature zero curvature at each end, which is appropriate for our fibrils, and by selecting certain modes, we can filter out contributions to the curvature from different effects. For example, cross-links can affect the modes with the lowest wavevectors, and tracking noise typically impacts the modes with the highest wavevectors.[17] We calculated the first 25 modes for the shape of each filament in every frame of the videos, which ensured that all informations were captured as the higher order modes quickly became dominated by experimental noise.

The average shape of the filament can be calculated by averaging the bending mode amplitudes, a_q, over time. This can then be used with the filament's length to reconstruct the tangent angle using eq 2. The reconstructed average tangent angle can then be used along with the average orientation and center of mass of the fibril to calculate the average position of the fibril, which is used to calculate the transverse displacement of the fibril away from its average position over time. Using the Fourier modes in this way allows us to avoid any potential errors from interpolating between points on the fibril contour which are output from the tracking algorithms. We calculated the transverse displacement, r, along each filament for each frame of the videos recorded, and this allowed us to calculate the effective confining potential, $V(r)$, a fibril experiences as a result of its local environment and physical properties. This was calculated from the probability distribution of the transverse displacement, $P(r)$, using the following equation for the confining potential in terms of the thermal energy, k_BT

$$V(r) = -k_BT \ln(P(r)) \tag{3}$$

which is based on Boltzmann statistics.[41] The confining potentials around representative filaments from four samples with different pNIPAM concentrations and temperatures are shown in Figure 3, and further similar images are shown in the Section 2 of the Supporting Information.

From the potentials in Figure 3, we can see that the fibrils move much more at 20 °C compared to 40 °C, even when there is no pNIPAM in the sample. Peptide self-assembly has been shown to be temperature dependent in the past and so it is not unusual for such systems to show temperature response.[42] All of the samples have similar confining potentials at 40 °C, whereas at the lower temperature, there is a more marked difference. At 20 °C, the pNIPAM concentrations of 1 and 8 mg/mL appear to restrict the motion of the I_3K fibrils somewhat, whereas when there is no pNIPAM or a high amount of pNIPAM (64 mg/mL), the motion is less restricted. In the high pNIPAM samples, the raw videos showed fibrils which were visibly more active than the other samples, and the fibrils appeared to be able to reptate and slide past each other much more easily.[43]

To quantitatively analyze the data from these potentials, we calculated the effective tube radius, which describes the range of transverse space that each section of each fibril can explore. To do this, we fitted the transverse potential with a Gaussian function and used the standard deviation of the Gaussian fit as

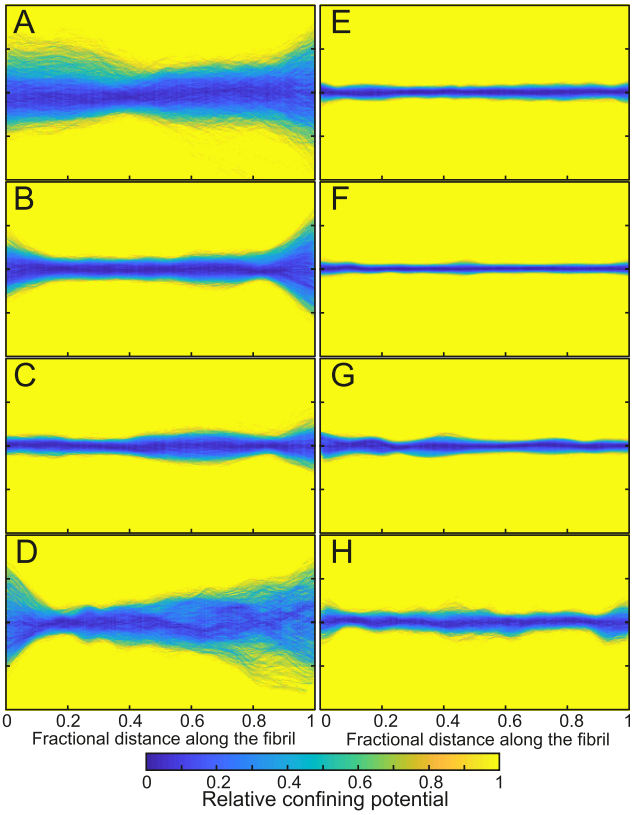

Figure 3. Transverse confining potential as a function of length along an I_3K filament from each of the different samples at 20 °C (A–D) and 40 °C (E–H). The fibril motion was damped for all samples at high temperature, whereas at the lower temperatures, the sample with no pNIPAM (A) and the sample with 64 mg/mL pNIPAM (D) showed large amplitude motion. The samples with 1 mg/mL (B) or 8 mg/mL (C) pNIPAM showed slightly damped motion at low temperatures. The lengths of the filaments were 30, 22, 20, 14, 17, 7, 26, and 11 μm for (A)–(H) respectively. The vertical scale represents the transverse distance away from the average position of the filament and goes from −0.5 to 0.5 μm. Three further plots for each sample are shown in the Section 2 of the Supporting Information.

the effective tube radius.[44] We calculated the tube radius every 50 nm along each fibril and then combined the results to provide the probability distribution of the tube radius for each sample. The results are shown for 20 and 40 °C in Figure 4A,B respectively.

The results in Figure 4 support the main conclusions from the potentials in Figure 3, and at the higher temperature all of the tube radii are very low. The distributions for the samples with 0, 1, and 8 mg/mL pNIPAM at 40 °C all peak at approximately 20 nm tube width, which is probably due to the tracking resolution of these kinds of experiments, i.e., the fibers are extensively cross-linked and thus move very little.[39,40] The 64 mg/mL pNIPAM sample peaks at a slightly higher value of approximately 40 nm. However, this is probably also due to the tracking resolution as the signal to noise ratio of these samples was significantly reduced due to the opacity of the sample at high pNIPAM concentrations (see Figure 1). Unfortunately, for the high-temperature sample, it appears as if almost all of the motions we observe are not measurable due to the resolution of our technique. After calculating the transverse velocity of fibrils from the different samples (see Section 1 of the Supporting Information), the fibrils are often moving at

DOI: 10.1021/acs.biomac.9b00085
Biomacromolecules 2019, 20, 1719–1730

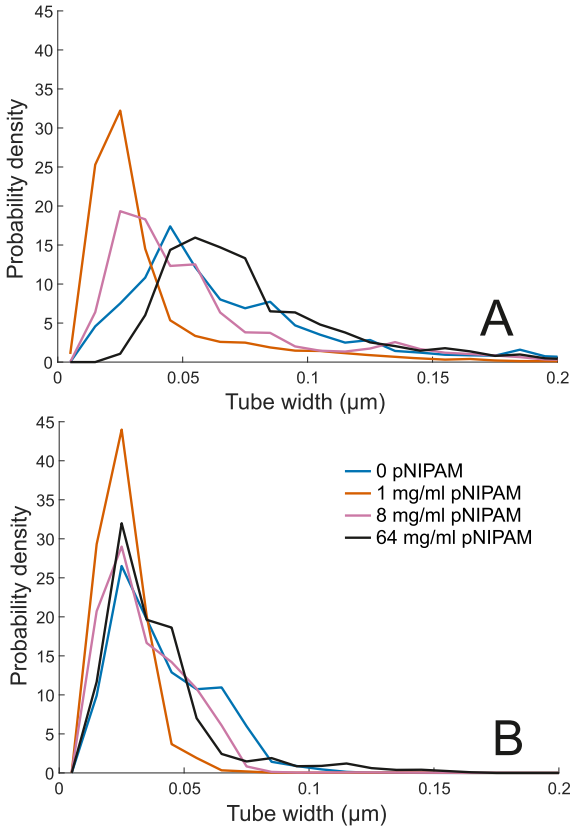

Figure 4. Tube widths from the dynamic data for each sample at 20 °C (A) and 40 °C (B). Increasing the temperature reduced the tube width for all samples. At high temperature (B), the peaks in the tube width are likely to be associated with the uncertainty in the measurements, which was approximately 25 nm, convolved with the actual movement of the fibril. In the cases of the 8 and 64 mg/mL pNIPAM samples at high temperature, imaging quality was reduced due to the opacity of the sample, which meant that tracking was less accurate and higher tube widths were recorded. The legend in (B) applies to both plots, and the data for each set is from the dynamics of 30−40 fibrils from two separately prepared samples.

greater than 2 μm/s, which would result in at least 20 nm of motion within the time taken to capture each frame. Therefore, the motion of the fibril over the 10 ms exposure time is enough to limit the tracking accuracy, and these kind of errors do routinely appear in other tracking techniques.[45]

For the lower temperature (Figure 4A), there are more significant differences between the samples. The addition of 1 mg/mL pNIPAM to the I_3K system appears to significantly damp the motion of the fibrils, and the resulting tube radius distribution is shifted such that there is rarely motion beyond 50 nm from the average fibril position. Further addition of pNIPAM allows the I_3K fibrils to move more freely, and the distribution widens and shifts to higher values of the tube radius for the 8 mg/mL pNIPAM sample and then again for the 64 mg/mL pNIPAM sample. With the highest amount of pNIPAM (64 mg/mL), the I_3K fibrils move more freely than when there was no pNIPAM in the sample, and the majority of fibrils have an effective tube radius of 50−100 nm. In our previous work, atomic force microscopy scans suggested that the pNIPAM was clustering onto the I_3K fibrils themselves, although this was for dried samples.[24] Thus, the higher mobility of fibrils at high pNIPAM concentrations might be due to the pNIPAM coating the outside of the peptide fibrils and reducing the possibility of cross-links between I_3K fibrils or a more indirect action due to increased osmotic swelling.

Returning to our model of the pNIPAM, modulating the osmotic pressure of the I_3K gel we can explain the behavior at lower temperatures. When the pNIPAM is below the LCST temperature and in its coil conformation, it can exert an extensional osmotic pressure on the I_3K network causing it to swell. This swelling will cause tension in the network, resulting in a change in the peptide fibril dynamics. Tension in the network will cause the amplitude of thermal oscillations to reduce significantly, as has been seen in the 1 mg/mL sample shown in Figure 3.[12,46,47] With a further increase of pNIPAM concentration to 8 and 64 mg/mL, the swelling causes cross-links in the network to break, allowing the fibrils to move more freely and explaining the increase in the effective tube radii for this samples. Crucially, only the parts of the fibrils which are actively connected to the network (i.e., have cross-links either side) will be under tension, and this allows the ends of fibrils to oscillate, as seen with the confining potential for a fibril in the 1 mg/mL pNIPAM sample in Figure 3B.

Another quantitative approach to understanding the dynamics is to look at the properties of the Fourier mode amplitudes, a_q, from eq 2. We calculated the mean-square difference (MSD) of the mode amplitudes as a function of lag time and then determined the plateau of the MSD, A_q, as a function of wavevector, q. For thermally equilibrated semiflexible filaments in a dilute phase, the MSD plateau is proportional to q^{-2} as the equipartition theorem can be used to show each mode contributes on average $\frac{1}{2}k_BT$ to the fibril bending energy.[39,40] The Fourier mode MSD plateaus, A_q, were calculated for each sample and fit to a power law to check the scaling with wavevector, and the results are shown in Section 3 of the Supporting Information. The result is as expected for the 20 °C sample with no pNIPAM, a scaling of -1.92 ± 0.07, close to the -2 expected for semiflexible filaments.[39,40] Furthermore, the fit gives a value of the persistence length of 2.1 ± 0.1 mm which is close to the value of 2.41 ± 0.07 mm found previously.[17] For the other samples, it appears as though the pNIPAM acts to damp the motion of lower wavelength modes and reduces the wavevector scaling.

Stress Modulation in the Networks. In our previous work on the dynamics of the I_3K system, we were able to provide strong evidence that states of prestress existed in fibrils of the gelled networks.[17] From the dramatic increases in the bulk mechanical properties and mobility of individual peptides, we deduce that it is due to a combination of changes in cross-link strength and density but also the prestresses the I_3K fibrils experience. From the microscopy images of the partially labeled network, it is clear that the temperature-induced coil-to-globule transition of the pNIPAM chains has a significant impact on the conformation of individual filaments, as shown in Figure 5. Figure 5 contains images of I_3K fibrils in the 8 mM I_3K network with 64 mg/mL pNIPAM. At 20 °C (Figure 5A), the fibrils appear very straight, without significant bending as one might expect for semiflexible filaments with a persistence length on the order of 2 mm. In contrast, Figure 5B,C contains images at 40 °C and show significant bending along the length of the filaments. Furthermore, the bends at the higher temperature appear to look like ripples along the fibrils, as if the fibril was at one point straight and has then been compressed axially, leading to a shape which is indicative of

DOI: 10.1021/acs.biomac.9b00085
Biomacromolecules 2019, 20, 1719−1730

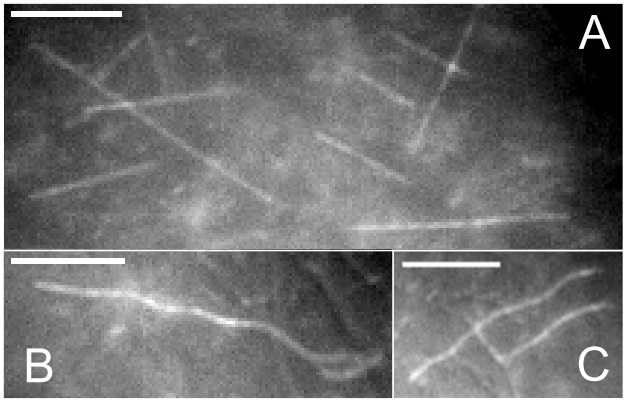

Figure 5. Fluorescence microscopy images of the partially labeled sample containing 8 mM I_3K and 64 mg/mL pNIPAM. At 20 °C (A), the fibrils all appear to be straight as would be expected from their 2 mm persistence length, whereas at 40 °C (B, C) the fibrils feature significant bending, much more than would be expected for their persistence length and they are therefore compressively stressed. The scale bar in all the images is 5 μm and the image depth of focus is approximately 200 nm.

confined buckling.[12] We measured the wavelength of the buckling, λ, present in Figure 5B and compared this with our values for the persistence length, L_p, and bulk elastic modulus of the network, G, according to the equation

$$\lambda = 2\pi\left(\frac{\kappa}{\alpha}\right)^{1/4} \tag{4}$$

where α depends on G, λ and the fiber radius, and $\alpha \sim 2.7G$ for I_3K. κ is the bending rigidity of the fibril and $\kappa = L_p k_B T$, where $k_B T$ is the thermal energy.[48] Using a persistence length of 2.1 mm and elastic modulus as 4.6 kPa, we obtain a buckling wavelength of approximately 1.0 μm, close to the calculated lambda of 2.9 μm from Figure 5B. This is in good agreement for a simple theory that neglects a range of nonlinear effects, such as frictional forces along the fibers. The minimum force required to induce a buckling instability, f_c, can also be calculated as $f_c = 2\sqrt{\kappa\alpha}$ and is ~0.7 nN, similar to the critical confined buckling force of microtubules in cells (~0.1 nN).[48] Overall, the images of confined buckling support our model. which predicts that the pNIPAM coil-to-globule transition leads to a reduction in osmotic pressure, which compresses and stiffens the I_3K network.

In our previous work on the states of prestress in the I_3K system, we applied a mixture model to the fibril bending energy distribution to separate the unstressed fibrils from those in a state of prestress (SPS).[17] Mixture models are popular in machine learning as they work well in classification problems when the subpopulations are overlapping.[49] However, one potential drawback of our previous method is that it only considered the marginal bending energy distribution, and any potential co-variance of the system on fibril length was neglected. For example, longer fibrils are likely to become stressed as they can sample more of the network, are in contact with more fibrils and thus are more likely to have multiple cross-links. To solve this problem, it could have been possible to generate a two-dimensional (2D) mixture model which attempted to fit the 2D probability distribution as a function of bending energy and contour length. However, as the functional form of each marginal distribution is complicated, it is unclear how the co-variance of the parameters should be included in the model. Alternatively, we attempted to model the 2D distribution using a Gaussian mixture model with various numbers of Gaussian profiles combining to fit the data. However, the models did not fit the fat-tailed data well and it seemed counter-intuitive to ignore the analytical expressions we had previously derived.[17] Therefore, to account for the co-variance, we developed an iterative, self-consistent procedure, which accounts for differences in the length distributions of the unstressed and stressed subpopulations within our data, built around fitting the marginal bending energy distribution.

To calculate the proportion of stressed fibrils in our sample, we used a mixture model to describe the bending energy distribution, $P_e(U)$

$$P_e(U) = \pi_u P_u(U) + \pi_s P_s(U) \tag{5}$$

where U is the bending energy and $P_u(U)$ and $P_s(U)$ are the bending energy distributions for the unstressed and stressed fibril subpopulations respectively. π_u and π_s describe the proportion of fibrils in each subpopulation and $\pi_u = 1 - \pi_s$, ensures the correct normalization. The I_3K fibrils have an equilibrium contour distribution which is exponential, as is common for systems of self-assembled filaments.[27,50] Assuming a power law scaling between the bending energy and contour length, we previously derived the bending energy of unstressed fibrils, $P_u(U)$, as

$$P_u(U) = (U_0^{1/\beta}\beta)^{-1}\frac{\exp\left(-\frac{U}{U_0}^{1/\beta}\right)}{U^{(\beta-1)/\beta}} \tag{6}$$

where U_0 and β are scaling parameters, which depend on the contour length distribution and the scaling between the bending energy and contour length.[17] Additionally, we were able to deduce that $P_s(U)$ was a Lévy distribution, given by

$$P_s(U) = \sqrt{\frac{c}{2\pi}}\frac{\exp\left(-\frac{c}{2(U-\mu)}\right)}{(U-\mu)^{3/2}} \tag{7}$$

where μ and c are the location and scale parameters for the distribution.

To find the states of prestress in our sample, the iterative mixture model proceeds in a similar manner to that from our previous work,[17] and the full procedure is shown in Figure 6. Initially, the length distribution of unstressed fibrils was assumed to be the same as the overall population of fibrils, i.e., exponential (step 1). We then generated a set of simulated dilute fibrils to match the unstressed length distribution based on a Monte Carlo simulation of dilute semiflexible polymer conformations (step 2). The bending energy distribution of these simulated fibrils was fit to find β and U_0 from eq 6 (step 3), and these values were then fixed (within error). Then, we used the mixture model (eq 5) to find π_u, π_s, μ, and c (step 4). At this point, we introduced a new step and calculated a weighting, w_f, for each fibril, f, which describes the ratio of $P_u(U_f)$ to $P_s(U_f)$

$$w_f = \frac{P_u(U_f)}{P_s(U_f)}\frac{1}{\sum w_f} \tag{8}$$

where U_f is the bending energy of the fibril and the weights were normalized such that they sum to 1. The weighting was used to allow the calculation of the length distribution of

DOI: 10.1021/acs.biomac.9b00085
Biomacromolecules 2019, 20, 1719−1730

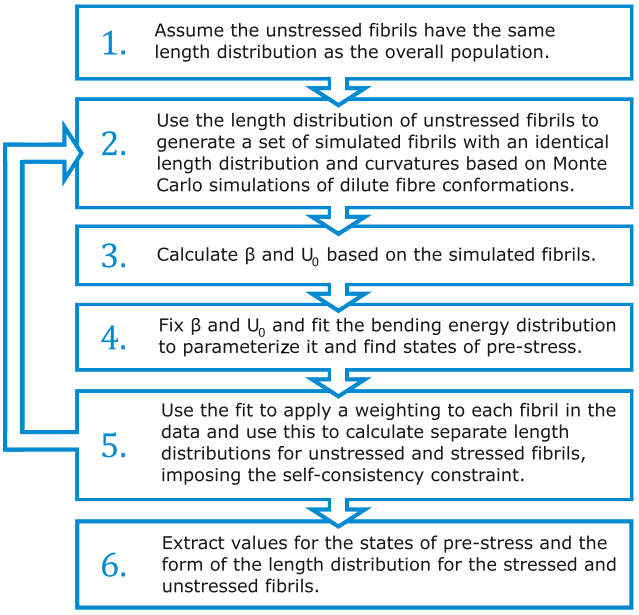

Figure 6. Schematic diagram of the fitting procedure in a self-consistent mixture model to find the states of prestress in the sample along with the length distributions for the stressed and unstressed fibrils. Steps 1−4 are identical to our previous work. We then weight each data point to generate length distributions for the stressed and unstressed fibrils in our sample. This allows us to refit the data with this refined length distribution and iterate steps 2−5 until convergence. Convergence is measured by the stability of the fit parameters between iterations.

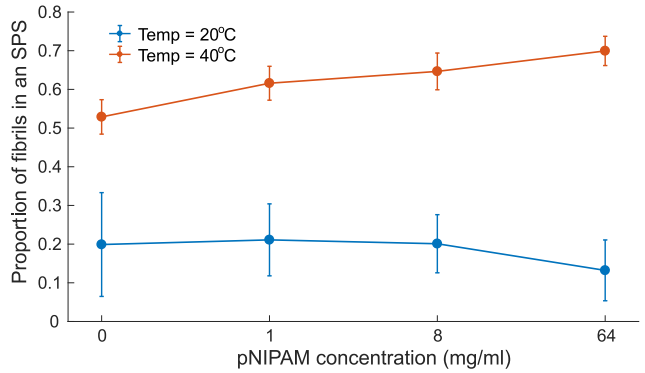

Figure 7. Proportion of I_3K fibrils in a state of prestress (SPS), as a function of pNIPAM concentration at different temperatures. As the pNIPAM concentration increased, the SPS in the I_3K fibrils decreased at low temperature and increased at high temperature, due to the different ways pNIPAM interacted with the I_3K above and below its critical temperature. The error bars are the uncertainty calculated from fitting to the mixture model for the bending energy distribution. The model was fit to the energy, and the length distributions formed from at least 600 fibers in each sample.

unstressed fibrils (step 5), equivalent to the marginal probability distribution on the length, $P(L) = \int P(U,L)\,dU$. The fitting procedure then returned to step 2 and used the new length distribution for unstressed fibrils in place of the previous one which originally assumed it would be the same as the overall population. Steps 2−5 were then repeated until convergence of the fit parameters for eq 5, which typically took less than five iterations.

By applying our self-consistent mixture model to the data from each of our samples, we calculated the proportion of I_3K fibrils in a state of prestress, as shown in Figure 7. In general, the data shows a similar trend to the rheology data from Figure 2B, with the increasing pNIPAM concentration causing an increase in stress at the higher temperature and a smaller effect at the lower temperature. However, in contrast to the rheology data, there is a significant difference in the I_3K sample with zero pNIPAM at different temperatures, and the states of prestress increased by a factor of 2.6 (0.20−0.52) as the temperature was increased. This increase in stress is consistent with our previous dynamics data (Figures 3 and 4), where the temperature increase dramatically reduced the effective tube widths for the I_3K chains alone. Once again, this is probably due to slight temperature-induced changes to the fibrils strengthening the cross-links between fibrils. In our previous work, we measured the states of prestress in I_3K fibrils at 10 mM concentration with pH 7 phosphate-buffered saline, which is a higher pH than that used here (pH 4) and therefore allowed stronger cross-links to be created due to a slightly less positive charge on the fibrils.[17] The proportion of states of prestress in these fibrils was 0.86, which is higher than we have measured here, suggesting that the temperature change from 20 to 40 °C induced a slight increase in cross-link strength but not to the levels of our previous work.

With the addition of pNIPAM, the effect of the temperature change is amplified compared to the I_3K alone. At the highest pNIPAM concentration, the states of prestress increase by a factor of 5.3, suggesting that the temperature change and the pNIPAM transition contribute equally (both a factor of ∼2.6). For all samples containing pNIPAM, there is a slight reduction in the states of prestress at low temperatures and a more significant increase in them at high temperature when compared to the I_3K only sample.

At low temperatures, the swollen gel is under tension, and currently our mixture model cannot calculate the tensional stress from the microscopy data. This is due to the large persistence length of the fibrils, which appear rod-like in many of images, and therefore it is difficult to distinguish whether they are under tension. As a result, there are no additional states of prestress for the low-temperature samples. However, there is also no significant reduction in the states of prestress, and this may be due to the inhomogeneous nature of these kinds of networks, causing local patches of stress to remain.[51] In the 64 mg/mL sample, the fibrils were very mobile and seemed disconnected from the network, suggesting that the extensional forces due to the pNIPAM's osmotic pressure were enough to break cross-links between fibrils.

At high temperatures, the addition of the pNIPAM causes a steady increase in the states of prestress in the I_3K network, in a similar fashion to the rheological data which demonstrated an increase in the elastic modulus on addition of pNIPAM (see Figure 2). The collapse of the pNIPAM chains exerts a compressional force on the I_3K network, which combined with the slightly stickier fibrils results in a high proportion of stressed fibrils. The sample with the most pNIPAM (64 mg/mL) shows a five-fold increase in the states of prestress in the sample following an increase in temperature from 20 to 40 °C. It also appears as if the neighboring filaments support one another and reduce the total failure of the fibrillar structure, resulting in enhanced mechanical properties. This is evident in the apparent confined buckling of fibrils shown in Figure 5 and

DOI: 10.1021/acs.biomac.9b00085
Biomacromolecules 2019, 20, 1719−1730

is a common phenomena found in other semiflexible filaments, such as microtubules.[48]

In general, it is misleading to directly compare the rheology results (Figure 2) with the proportion of pre-stressed fibrils (Figure 7). First of all, the shear modulus can take a very wide range of positive values, whereas the proportion of stressed fibrils is limited between 0 and 1. Therefore, it is not clear how they are interdependent. Studies on collagen suggest that more stress equates to a higher shear modulus,[18] but the peptide network is complex and inhomogeneous so it is not obvious what the scaling would be. From our results, the states of prestress do not significantly affect the bulk properties when the proportion of stressed fibrils is less than ~0.6, as the zero pNIPAM sample increases in SPS, but does not change significantly in shear modulus. This may be because the stress cannot percolate through the network and is limited to local regions or individual fibrils. At higher proportions of stressed fibrils, such as the 64 mg/mL sample at 40 °C, the stress may be able to percolate causing states of self-stress to appear, which are a network property. This may more strongly modulate the overall network properties, as local regions of stress become interconnected and dominate the network.

Another result of our model is the length distributions of the stressed and unstressed fibrils in each sample. The probability density of each length distribution is shown in Figure 8, allowing the effect of the temperature change to be observed. For each of the distributions, we calculated the mean and standard deviation, and the results are shown in Figure 8E,F, respectively. The results do not show a strong dependence on the pNIPAM concentration, but there is a clear difference between the stressed and unstressed fibrils, and the stressed fibrils are significantly longer than the unstressed ones. At 40 °C, the distributions shift slightly toward shorter fibril lengths, and there are very few unstressed fibrils above 10 μm in length at this temperature. The stressed fibrils have a broader distribution with a standard deviation from 4 to 6 μm compared to the unstressed fibrils from 2 to 4 μm. The stressed fibrils at 40 °C show the strongest dependence on pNIPAM concentration, and the mean for this population decreases with increasing pNIPAM concentration. The overall length distribution for the fibrils is exponential, so as the mean of the stressed fibril distribution reduces it incorporates more and more short fibrils (which are most numerous overall), resulting in a reduced standard deviation. This shows that the increased pNIPAM concentration causes stress to be distributed among a wider range of fibril in the 8 and 64 mg/mL pNIPAM samples.

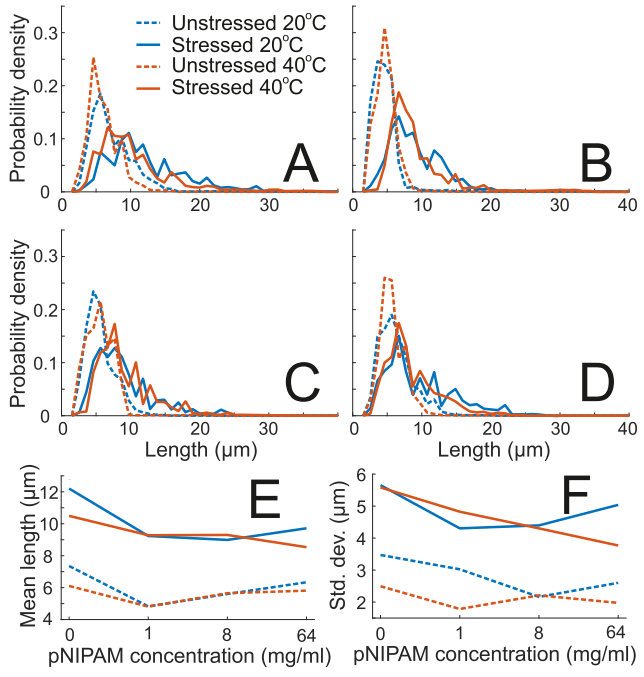

Figure 8. (A–D) Probability density of fibril lengths for I_3K fibrils which are either stressed or unstressed from the self-consistent mixture model (Figure 7). The distributions are shown for the high- and low-temperatures studied and at pNIPAM concentrations of 0, 1, 8, and 64 mg/mL in subplots (A), (B), (C), and (D) respectively. The largest temperature effect seems to be for the 0 and 64 mg/mL pNIPAM concentrations, where fibrils >10 μm in length all become stressed at the higher temperatures. From all of the figures, it is seen that the longer fibers have a substantially higher probability to be in a state of prestress. The mean and standard deviation of each length distribution are shown in (E) and (F). The legend in (A) applies to all of the subplots.

Along with the effect of the temperature change on each sample, we can also draw more general conclusions about the system from Figure 8. For example, the smaller unstressed populations at high temperatures in all samples relates to fibrils which are not active in the network, i.e., have one or less cross-links. In the classical literature on flexible polymer gels, these are called dangling ends and do not directly contribute to the elasticity of the networks.[52]

Through analysis of network dynamics using bulk rheology and fluorescence microscopy of individual peptide chains we can visualize the osmotic pressure model as shown in Figure 9. The I_3K only system features populations of unstressed and stressed fibrils which are compressed due to cross-links with the network preventing them from relaxing and trapping them in states of quenched disorder (Figure 9A). The addition of pNIPAM at low temperatures (<32 °C) swells the network and introduces tension to some I_3K fibrils, weakening the network. However, many of the quenched disorder states persist as inhomogeneities and cross-links in the network remain, trapping certain fibrils in states of prestress (Figure 9B). Above the LCST of pNIPAM (>32 °C), the pNIPAM has reduced in volume by 3 orders of magnitude, reversing the osmotic pressure and compressing the I_3K network. This leads to additional cross-links between the fibrils, a high proportion of fibrils in compressive states of prestress and confined buckling events in certain cases (Figure 9C). These changes in the osmotic pressure and states of prestress are closely linked with significant changes in the systems' bulk mechanical properties of up to 3 orders of magnitude (Figure 2) and as such are extremely important for the design of materials based on semiflexible polymer gels and networks. Although we have shown these changes exist, we have not yet been able to fully describe the system's response in terms of analytical models for how states of prestress and the shear modulus are linked, which is an important next step. This could then create an opportunity for the control of a wide range of material properties on the nanoscale, which are crucial for many biomimetic applications, such as adhesion, mechanics, phase separation, viscoelasticity, sol/gel transition and fracture.[53] We have shown the temperature dependent behavior using pNIPAM but this could potentially be enhanced/tuned further using other thermoresponsive polymers such as Pluronic F127, which can gel independently.[54] Alongside temperature control,

DOI: 10.1021/acs.biomac.9b00085
Biomacromolecules 2019, 20, 1719–1730

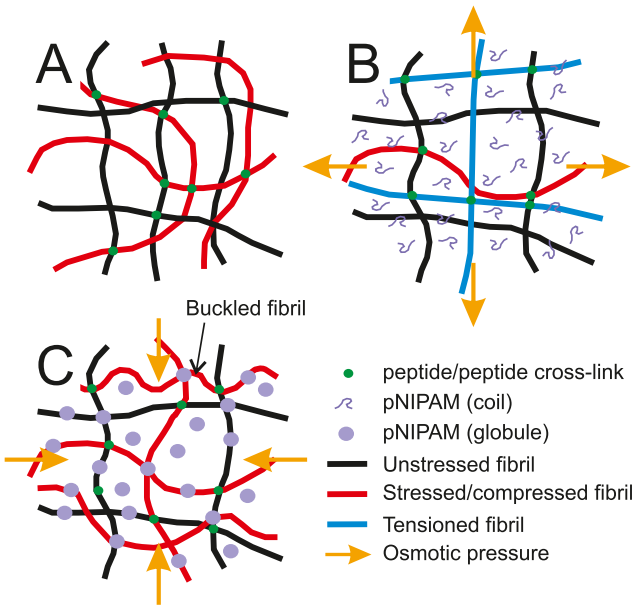

Figure 9. Schematic diagrams of the I_3K/pNIPAM networks in various conditions (not to scale). (A) The I_3K system alone with no pNIPAM. Some of the fibrils are stressed due to the forces imposed by cross-links and others are not. (B) The I_3K/pNIPAM network below the pNIPAM lower critical solution temperature (LCST) features osmotic swelling due to the pNIPAM and causes some I_3K fibrils to be under tension. This causes a weakening of cross-links and a reduction in the mechanical strength of the network. (C) The I_3K/pNIPAM network above the pNIPAM LCST features osmotic compression as the pNIPAM shrinks during the coil-to-globule transition. This strengthens the network and causes some I_3K fibrils to buckle.

the use of light and electric potentials have also been shown to modulate self-assembly processes and could also be used to actuate stress in these networks[55−57]

Additional work is needed to fully understand the impacts of osmotic stress, such as through dehydration, on the fibers within these kinds of gels and further investigation could proceed through microscopy combined with shear cell rheometry[58] In addition, through careful experiment design and temperature control, the coil−globule transition of pNIPAM in the peptide networks could be visualized using these kinds of experiment. Furthermore, when similar peptide-based gels designed for therapeutics are put into use, they will inevitably have to withstand the range of osmotic pressures exerted on them by the various environments present *in vivo*. We have shown how these forces can drastically impact the peptide gel network, and so further study of these effects is necessary to provide higher performance therapeutic biomaterials. The local stress environment presented by these materials will closely impact the behavior of bacteria and biofilm development around these materials, and managing these types of interactions is a major challenge for modern healthcare.[59] Future work is also needed to investigate how osmotic stress modulates the number of fibers in states of prestress in naturally occurring biopolymer networks, such as *in vivo* systems implicated in amyloid diseases like Alzheimer's and Parkinson's.[60]

CONCLUSIONS

We used a combination of bulk rheology and image analysis of the dynamics of individual peptide fibrils through single-molecule fluorescence microscopy to demonstrate active modulation of peptide gel mechanics through the control of osmotic pressures. We combined the thermoresponsive polymer pNIPAM with the self-assembling synthetic peptide I_3K to form a hybrid system capable of a temperature-controlled sol−gel transition, with changes in the elastic modulus of up to 3 orders of magnitude (1 Pa to 4.6 kPa). The addition of the pNIPAM to the I_3K gel at low temperatures resulted in a lowering of the elastic modulus and an increase in the scaling between elastic modulus and frequency, suggesting that the system was acting as a solution of semiflexible filaments and that a sol−gel transition has occurred. However, the dynamics of the peptides shows that the addition of low to moderate amounts of pNIPAM (1 and 8 mg/mL) actually reduced the amplitude of thermal fluctuations at low temperatures with respect to the I_3K alone. As the peptide is self-assembled prior to the addition of pNIPAM, we believe that this phenomenon is due to an extensional osmotic pressure exerted by the pNIPAM coils on the I_3K network. This would cause the fibrils to be under tension, which greatly reduces the amplitude of thermal oscillations.[12,46] When a high amount of pNIPAM is introduced, the cross-links are broken by this tension, causing the I_3K fibrils to have dynamics similar to reptation in a semidilute entangled solution. At higher temperatures, the pNIPAM undergoes a coil-to-globule transition, which decreases its volume by 3 orders of magnitude, causing a reversal of the osmotic pressure and a compressive force on the I_3K network. This causes a large increase in the mechanical strength of the network (hardening), and the fibrils show signs of confined buckling in some samples, with rippled shapes. In addition, the pNIPAM has been shown to interact directly with the peptide fibers in our other work.[24] These interactions are likely to modulate the cross-links of the load bearing peptide network and co-operate with the osmotic forces to produce a bulk material with enhanced properties.

We also performed analysis of the fibril's shape to deduce the states of prestress in the networks under different conditions. We developed a self-consistent iterative mixture model which can account for differences between the length distributions of stressed and unstressed fibrils. This showed that the temperature switch can also be used to control the states of prestress in the peptide network. The I_3K only network also features a temperature dependence, and the stresses within it increase significantly at higher temperatures. We have demonstrated that states of prestress in I_3K can be modulated by the thermoresponsive polymer pNIPAM to actively control the bulk and meso-scale properties of the I_3K fibril network. These results are applicable to commercially relevant therapeutic biomaterials and other naturally occurring biopolymer networks, such as microtubules and amyloid fibrils, in neurodegenerative diseases such as Alzheimer's and Parkinson's disease.

ASSOCIATED CONTENT

Supporting Information

The Supporting Information is available free of charge on the ACS Publications website at DOI: 10.1021/acs.biomac.9b00085.

DOI: 10.1021/acs.biomac.9b00085
Biomacromolecules 2019, 20, 1719−1730

Fibril tracking procedure and transverse velocity profiles (Section 1); additional fibril confining potentials (Section 2); analysis of dynamics using Fourier mode amplitudes (Section 3) (PDF)

AUTHOR INFORMATION

Corresponding Authors

*E-mail: t.a.waigh@manchester.ac.uk (T.A.W.).
*E-mail: j.lu@manchester.ac.uk (J.R.L.).

ORCID

Henry Cox: 0000-0002-6815-1097
Meiwen Cao: 0000-0002-3072-6780
Hai Xu: 0000-0002-5796-4404
Thomas A. Waigh: 0000-0002-7084-559X
Jian R. Lu: 0000-0001-5648-3564

Notes

The authors declare no competing financial interest.

ACKNOWLEDGMENTS

We thank Viki Allan, James Sanders, and Mark Dickinson for helping with the construction of the STORM equipment and EPSRC for funding this project under the Ph.D. studentship to H.C. and also under an MRC research grant (EP/F062966/1).

REFERENCES

(1) Hamley, I. W. Small bioactive peptides for biomaterials design and therapeutics. *Chem. Rev.* **2017**, *117*, 14015−14041.
(2) Chen, C.; Zhang, Y.; Fei, R.; Cao, C.; Wang, M.; Wang, J.; Bai, J.; Cox, H.; Waigh, T.; Lu, J. R.; Xu, H. Hydrogelation of the short self-assembling peptide I3QGK regulated by transglutaminase and use for rapid hemostasis. *ACS Appl. Mater. Interfaces* **2016**, *8*, 17833−17841.
(3) Raymond, D. M.; Nilsson, B. L. Multicomponent peptide assemblies. *Chem. Soc. Rev.* **2018**, *47*, 3659−3720.
(4) Bakota, E. L.; Aulisa, L.; Galler, K. M.; Hartgerink, J. D. Enzymatic cross-linking of a nanofibrous peptide hydrogel. *Biomacromolecules* **2011**, *12*, 82−87.
(5) DiMaio, J. T.; Doran, T. M.; Ryan, D. M.; Raymond, D. M.; Nilsson, B. L. Modulating supramolecular peptide hydrogel viscoelasticity using biomolecular recognition. *Biomacromolecules* **2017**, *18*, 3591−3599.
(6) Gong, J. P. Why are double network hydrogels so tough? *Soft Matter* **2010**, *6*, 2583.
(7) Djabourov, M.; Nishinari, K.; Ross-Murphy, S. B. *Physical Gels from Biological and Synthetic Polymers*; Cambridge University Press: Cambridge, 2011.
(8) Li, J.; Celiz, A. D.; Yang, J.; Yang, Q.; Wamala, I.; Whyte, W.; Seo, B. R.; Vasilyev, N. V.; Vlassak, J. J.; Suo, Z.; Mooney, D. J. Tough adhesives for diverse wet surfaces. *Science* **2017**, *357*, 378−381.
(9) Zhang, S. Fabrication of novel biomaterials through molecular self-assembly. *Nat. Biotechnol.* **2003**, *21*, 1171−1178.
(10) Wang, J.; Liu, K.; Xing, R.; Yan, X. Peptide self-assembly: Thermodynamics and kinetics. *Chem. Soc. Rev.* **2016**, *45*, 5589−5604.
(11) Hamley, I. W. Peptide fibrillization. *Angew. Chem., Int. Ed.* **2007**, *46*, 8128−8147.
(12) Broedersz, C. P.; Mackintosh, F. C. Modeling semiflexible polymer networks. *Rev. Mod. Phys.* **2014**, *86*, 995−1036.
(13) Loo, Y.; Zhang, S.; Hauser, C. A. E. From short peptides to nanofibers to macromolecular assemblies in biomedicine. *Biotechnol. Adv.* **2012**, *30*, 593−603.
(14) Hibbeler, R. C. *Structural Analysis*; Pearson: Singapore, 2004.
(15) Huisman, E. M.; Lubensky, T. C. Internal stresses, normal modes, and nonaffinity in three-dimensional biopolymer networks. *Phys. Rev. Lett.* **2011**, *106*, No. 088301.
(16) Lubensky, T. C.; Kane, C. L.; Mao, X.; Souslov, A.; Sun, K. Phonons and elasticity in critically coordinated lattices. *Rep. Prog. Phys.* **2015**, *78*, No. 073901.
(17) Cox, H.; Xu, H.; Waigh, T. A.; Lu, J. R. Single-molecule study of peptide gel dynamics reveals states of prestress. *Langmuir* **2018**, *34*, 14678−14689.
(18) Licup, A. J.; Münster, S.; Sharma, A.; Sheinman, M.; Jawerth, L. M.; Fabry, B.; Weitz, D. A.; MacKintosh, F. C. Stress controls the mechanics of collagen networks. *Proc. Natl. Acad. Sci. U.S.A.* **2015**, *112*, 9573−9578.
(19) Wang, X.; Qiu, X.; Wu, C. Comparison of the coil-to-globule and the globule-to-coil transitions of a single poly(N-isopropylacrylamide) homopolymer chain in water. *Macromolecules* **1998**, *31*, 2972−2976.
(20) Senff, H.; Richtering, W. Temperature sensitive microgel suspensions: colloidal phase behavior and rheology of soft spheres. *J. Chem. Phys.* **1999**, *111*, 1705−1711.
(21) Maslovskis, A.; Guilbaud, J. B.; Grillo, I.; Hodson, N.; Miller, A. F.; Saiani, A. Self-assembling peptide/thermoresponsive polymer composite hydrogels: effect of peptide-polymer interactions on hydrogel properties. *Langmuir* **2014**, *30*, 10471−10480.
(22) Conley, G. M.; Nöjd, S.; Braibanti, M.; Schurtenberger, P.; Scheffold, F. Super-resolution microscopy of the volume phase transition of pNIPAM microgels. *Colloids Surf., A* **2016**, *499*, 18−23.
(23) Bromberg, L. E.; Ron, E. S. Temperature-responsive gels and thermogelling polymer matrices for protein and peptide delivery. *Adv. Drug Delivery Rev.* **1998**, *31*, 197−221.
(24) Cao, M.; Wang, Y.; Hu, X.; Gong, H.; Li, R.; Cox, H.; Waigh, T. A.; Xu, H.; Lu, J. R. Reversible thermosensitive peptide/PNIPAM hydrogels for controlled drug delivery, submitted for publication, 2019.
(25) Xu, H.; Wang, Y.; Ge, X.; Han, S.; Wang, S.; Zhou, P.; Shan, H.; Zhao, X.; Lu, J. R. Twisted nanotubes formed from ultrashort amphiphilic peptide I3K and their templating for the fabrication of silica nanotubes. *Chem. Mater.* **2010**, *22*, 5165−5173.
(26) Cao, M.; Wang, Y.; Ge, X.; Cao, C.; Wang, J.; Xu, H.; Xia, D.; Zhao, X.; Lu, J. R. Effects of anions on nanostructuring of cationic amphiphilic peptides. *J. Phys. Chem. B* **2011**, *115*, 11862−11871.
(27) Cox, H.; Georgiades, P.; Xu, H.; Waigh, T. A.; Lu, J. R. Self-assembly of mesoscopic peptide surfactant fibrils investigated by STORM super-resolution fluorescence microscopy. *Biomacromolecules* **2017**, *18*, 3481−3491.
(28) Costa, D.; Graça Miguel, M.; Lindman, B. Effect of additives on swelling of covalent DNA gels. *J. Phys. Chem. B* **2007**, *111*, 8444−8452.
(29) Kim, W. K.; Moncho-Jordá, A.; Roa, R.; Kanduč, M.; Dzubiella, J. Cosolute partitioning in polymer networks: effects of flexibility and volume transitions. *Macromolecules* **2017**, *50*, 6227−6237.
(30) Gao, J.; Tang, C.; Elsawy, M. A.; Smith, A. M.; Miller, A. F.; Saiani, A. Controlling self-assembling peptide hydrogel properties through network topology. *Biomacromolecules* **2017**, *18*, 826−834.
(31) Bai, J.; Chen, C.; Wang, J.; Zhang, Y.; Cox, H.; Zhang, J.; Wang, Y.; Penny, J.; Waigh, T.; Lu, J. R.; Xu, H. Enzymatic regulation of self-assembling peptide A9K2 nanostructures and hydrogelation with highly selective antibacterial activities. *ACS Appl. Mater. Interfaces* **2016**, *8*, 15093−15102.
(32) Chu, E. K.; Kilic, O.; Cho, H.; Groisman, A.; Levchenko, A. Self-induced mechanical stress can trigger biofilm formation in uropathogenic Escherichia coli. *Nat. Commun.* **2018**, *9*, No. 4087.
(33) Smith, M. B.; Li, H.; Shen, T.; Huang, X.; Yusuf, E.; Vavylonis, D. Segmentation and tracking of cytoskeletal filaments using open active contours. *Cytoskeleton* **2010**, *67*, 693−705.
(34) Usov, I.; Mezzenga, R. FiberApp: an open-source software for tracking and analyzing polymers, filaments, biomacromolecules, and fibrous objects. *Macromolecules* **2015**, *48*, 1269−1280.
(35) Morse, D. C. Viscoelasticity of concentrated isotropic solutions of semiflexible polymers. 2. Linear response. *Macromolecules* **1998**, *31*, 7044−7067.

DOI: 10.1021/acs.biomac.9b00085
Biomacromolecules 2019, 20, 1719−1730

(36) Broedersz, C. P.; Depken, M.; Yao, N. Y.; Pollak, M. R.; Weitz, D. A.; MacKintosh, F. C. Cross-link-governed dynamics of biopolymer networks. *Phys. Rev. Lett.* **2010**, *105*, No. 238101.
(37) Tanaka, T.; Sato, E.; Hirokawa, Y.; Hirotsu, S.; Peetermans, J. Critical kinetics of volume phase transition of gels. *Phys. Rev. Lett.* **1985**, *55*, 2455−2458.
(38) Rubinstein, M.; Colby, R. H. *Polymer Physics*; Oxford University Press, 2003.
(39) Brangwynne, C. P.; Koenderink, G. H.; Barry, E.; Dogic, Z.; MacKintosh, F. C.; Weitz, D. A. Bending dynamics of fluctuating biopolymers probed by automated high-resolution filament tracking. *Biophys. J.* **2007**, *93*, 346−359.
(40) Gittes, F.; Mickey, B.; Nettleton, J.; Howard, J. Flexural rigidity of microtubules and actin filaments measured from thermal fluctuations in shape. *J. Cell Biol.* **1993**, *120*, 923−934.
(41) Keshavarz, M.; Engelkamp, H.; Xu, J.; Van Den Boomen, O. I.; Maan, J. C.; Christianen, P. C.; Rowan, A. E. Confining potential as a function of polymer stiffness and concentration in entangled polymer solutions. *J. Phys. Chem. B* **2017**, *121*, 5613−5620.
(42) Löwik, D. W. P. M.; Leunissen, E. H. P.; van den Heuvel, M.; Hansen, M. B.; van Hest, J. C. M. Stimulus responsive peptide based materials. *Chem. Soc. Rev.* **2010**, *39*, 3394−3412.
(43) Käs, J.; Strey, H.; Sackmann, E. Direct imaging of reptation for semiflexible actin-filaments. *Nature* **1994**, *368*, 226−229.
(44) Lattanzi, G.; Munk, T.; Frey, E. Transverse fluctuations of grafted polymers. *Phys. Rev. E* **2004**, *69*, No. 021801.
(45) Jahnel, M.; Waigh, T. A.; Lu, J. R. Thermal fluctuations of fibrin fibres at short time scales. *Soft Matter* **2008**, *4*, 1438.
(46) Granek, R. From semi-flexible polymers to membranes: anomalous diffusion and reptation. *J. Phys. II* **1997**, *7*, 1761−1788.
(47) Georgiades, P.; Allan, V. J.; Wright, G. D.; Woodman, P. G.; Udommai, P.; Chung, M. A.; Waigh, T. A. The flexibility and dynamics of the tubules in the endoplasmic reticulum. *Sci. Rep.* **2017**, *7*, No. 16474.
(48) Brangwynne, C. P.; MacKintosh, F. C.; Kumar, S.; Geisse, N. A.; Talbot, J.; Mahadevan, L.; Parker, K. K.; Ingber, D. E.; Weitz, D. A. Microtubules can bear enhanced compressive loads in living cells because of lateral reinforcement. *J. Cell Biol.* **2006**, *173*, 733−741.
(49) Bishop, C. M. *Pattern Recognition and Machine Learning*; Springer, 2006.
(50) Cohen, S. I. A.; Vendruscolo, M.; Dobson, C. M.; Knowles, T. P. J. Nucleated polymerization with secondary pathways. III. Equilibrium behavior and oligomer populations. *J. Chem. Phys.* **2011**, *135*, No. 065107.
(51) Didonna, B. A.; Lubensky, T. C. Nonaffine correlations in random elastic media. *Phys. Rev. E* **2005**, *72*, 1−23.
(52) de Gennes, P. G. *Scaling Concepts in Polymer Physics*; Cornell University Press, 1980.
(53) Sato, K.; Hendricks, M. P.; Palmer, L. C.; Stupp, S. I. Peptide supramolecular materials for therapeutics. *Chem. Soc. Rev.* **2018**, 7539−7551.
(54) Prud'homme, R. K.; Wu, G.; Schneider, D. K. Structure and rheology studies of poly(oxyethylene-oxypropylene-oxyethylene) aqueous solution. *Langmuir* **1996**, *12*, 4651−4659.
(55) Xue, B.; Qin, M.; Wang, T.; Wu, J.; Luo, D.; Jiang, Q.; Li, Y.; Cao, Y.; Wang, W. Electrically controllable actuators based on supramolecular peptide hydrogels. *Adv. Funct. Mater.* **2016**, *26*, 9053−9062.
(56) Li, X.; Fei, J.; Xu, Y.; Li, D.; Yuan, T.; Li, G.; Wang, C.; Li, J. A photoinduced reversible phase transition in a dipeptide supramolecular assembly. *Angew. Chem., Int. Ed.* **2018**, *57*, 1903−1907.
(57) Xing, R.; Yuan, C.; Li, S.; Song, J.; Li, J.; Yan, X. Charge-induced secondary structure transformation of amyloid-derived dipeptide assemblies from β-sheet to α-helix. *Angew. Chem., Int. Ed.* **2018**, *57*, 1537−1542.
(58) Kirchenbuechler, I.; Guu, D.; Kurniawan, N. A.; Koenderink, G. H.; Lettinga, M. P. Direct visualization of flow-induced conformational transitions of single actin filaments in entangled solutions. *Nat. Commun.* **2014**, *5*, No. 5060.
(59) Hall-Stoodley, L.; Costerton, J. W.; Stoodley, P. Bacterial biofilms: from the natural environment to infectious diseases. *Nat. Rev. Microbiol.* **2004**, *2*, 95−108.
(60) Schleeger, M.; Vandenakker, C. C.; Deckert-Gaudig, T.; Deckert, V.; Velikov, K. P.; Koenderink, G.; Bonn, M. Amyloids: from molecular structure to mechanical properties. *Polymer* **2013**, *54*, 2473−2488.

DOI: 10.1021/acs.biomac.9b00085
Biomacromolecules 2019, 20, 1719−1730